43rd Annual Symposium on Frequency Control - 1989

VELOCITY DISTRIBUTIONS FROM THE FOURIER TRANSFORMS OF RAMSEY LINE SHAPES

Jon H. Shirley
Consultant to Time and Frequency Division
National Institute of Standards and Technology
Boulder, CO 80303

Abstract

A computerized method for finding velocity distributions from the Fourier transforms of Ramsey line shapes has been developed. Since atoms in certain velocity groups (those returning to their initial state) do not contribute to the lineshape, a single lineshape transform gives an incomplete picture of the velocity distribution. To bypass this problem we use Ramsey lineshape data taken at different excitation powers so that these velocity groups will contribute. A weighted average of data from three powers gives satisfactory results. The excitation amplitude parameter b is found by minimizing a quality-of-fit criterion. The method is limited to long standards by the assumption that the excitation length ℓ is much less than the drift region length L. However, the addition of first order ℓ/L corrections to the theory make the method usable for shorter standards. The method has been tested with lineshapes theoretically generated from known velocity distributions.

I. Introduction

The advent of optically pumped cesium beams [1] promises to improve the accuracy of primary frequency standards. But knowledge of the velocity distribution must also be improved to evaluate adequately systematic errors, particularly the second-order Doppler effect. Existing methods of obtaining velocity distributions based on pulsed excitation [2,3] or microwave power variation [4] have limitations in the precision of the experimental data. Measurement of Ramsey lineshapes can be done with greater precision, but the published method for extracting velocity distributions from lineshapes [5] is complex in theory and sometimes ambiguous in application.

We have developed an alternate method for finding velocity distributions that takes advantage of the large L/ℓ ratios found in primary standards. The idea for our method appears in a paper by Daams [6]. His analysis applies at one power. The need for lineshapes at different powers to obtain a complete velocity distribution was known by Jarvis [5] and will be further explained here.

II. Description of the Fourier Transform Method for $\ell \ll L$

A. Basic Theory

When the detuning is small enough to reveal only the Ramsey fringe pattern and not the shape of the underlying Rabi pedestal, the transition probability can be represented by [7, Eq. (V.38)]

$$P(\lambda) = \int_0^\infty \rho(T)\sin^2 2b\tau \cos^2 \tfrac{1}{2}\lambda T \, dT. \qquad (1)$$

Here $\tau = \ell/v$ and $T = L/v$ are the transit times for an atom of velocity v across the excitation and drift regions respectively, b is the Rabi frequency proportional to the microwave field strength, and $\lambda = \omega - \omega_0$ is the detuning of the exciting frequency ω from the atomic resonance frequency ω_0. The $\sin^2 2b\tau$ factor represents the Rabi excitation probability for the two excitation regions (without a drift region), while the $\cos^2 \tfrac{1}{2}\lambda T$ factor introduces the interference developed during the drift time by a mistuning of the excitation frequency. The atomic velocity average is represented by the integral over the distribution $\rho(T)$ of drift region transit times T. If we use the half-angle formula to expand the interference factor, we obtain

$$P(\lambda) = \tfrac{1}{2}R(0) + \tfrac{1}{2}R(\lambda), \qquad (2)$$

where

$$R(\lambda) = \int_0^\infty \rho(T) \sin^2 aT \cos \lambda T \, dT \qquad (3)$$

is the Ramsey fringe pattern and R(0) is the Rabi pedestal, constant over the range of detuning considered. We have also introduced $a = 2b\ell/L$ so that $2b\tau$ can be abbreviated by aT. For a distribution $\rho(T)$ of finite width, $R(\lambda)$ tends to zero for large λ.

From (3), $R(\lambda)$ is the Fourier cosine transform of the product of ρ and the transition probability. This product can be interpreted as the distribution of transit times for atoms which would make a transition were there no drift region. The transition probability factor depresses $\rho(T)$ a little where $\sin^2 aT$ is large, and a lot where $\sin^2 aT$ is small (see Fig. 1). The point T_m where the

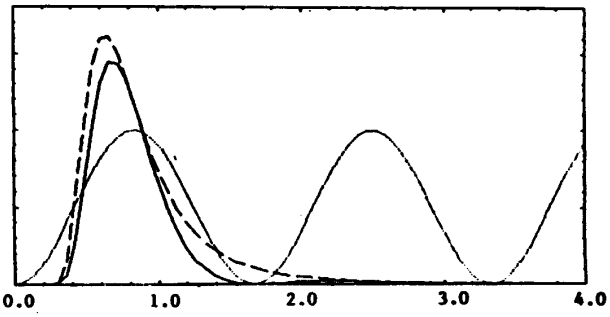

Fig. 1 The full thermal velocity distribution (dashed line), the transition probability factor $\sin^2 aT$ (dotted line), and their product (solid line). The horizontal scale is in units of $\alpha T/L$ where α is the most probable velocity in the source oven [7].

product first goes to zero provides a measure of the parameter a (or b) since $T_m = \pi/a$. Atoms having a transit time of T_m, $2T_m$, $3T_m$... have exactly returned to their initial state, hence do not contribute to the lineshape.

This Fourier transform picture helps explain the power dependence of Ramsey lineshapes. At lower powers the period of $\sin^2 aT$ increases and the product is peaked at higher T values than $\rho(T)$. The transform then oscillates more rapidly making a narrower lineshape. Similarly, at higher powers the product peaks at lower T values leading to a broader lineshape. At powers much above optimum $\sin^2 aT$ may divide $\rho(T)$ into a two-peaked function. The Ramsey fringe will then show the beating of two oscillation frequencies.

If we perform a numerical Fourier transform of a Ramsey fringe and attempt to divide out $\sin^2 aT$ to obtain $\rho(T)$, we encounter two problems. The first is illustrated in Fig. 2. The transform does

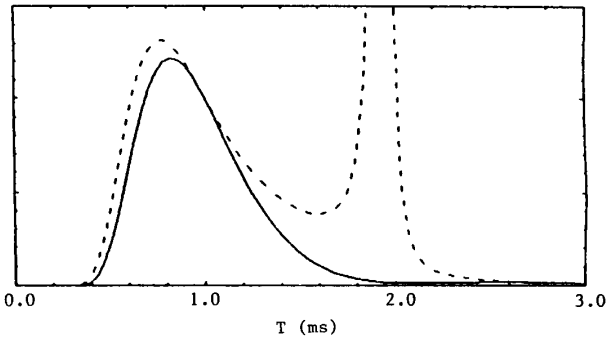

Fig. 2 Fourier transform of a Ramsey lineshape (solid curve) and trial value for $\rho(T)$ (broken curve) obtained by dividing out $\sin^2 aT$ everywhere.

not actually go to zero at T_m, $2T_m$,... Hence when we divide by small numbers we obtain large numbers. The second problem is that a (or T_m) is usually not well known, so $\sin^2 aT$ cannot be accurately evaluated. Both problems are solved in the next section.

B. Use of Multiple Ramsey Lineshapes

The transform of a single Ramsey pattern gives an incomplete picture of $\rho(T)$ since the $\sin^2 aT$ factor suppresses information about $\rho(T)$ near T_m, $2T_m$, $3T_m$.... To complete the picture we use Ramsey fringe data at different levels of microwave excitation power (a or b values). The transforms of this data then have different $\sin^2 aT$ factors corresponding to different regions of $\rho(T)$ being suppressed.

To visualize these regions suppose we reject data for which $\sin^2 aT$ is less than 0.25. Then a single Ramsey fringe pattern at optimum power gives us information about $\rho(T)$ only over those regions in T covered by the black bars in the first row of Fig. 3. The first bar includes the region around $\frac{1}{2}T_m$ where $\rho(T)$ has its maximum. But a broad distribution extends much further than the first bar. To fill in the gaps in the first row we try other power levels. Data taken at a power level 3 dB above optimum (b larger by a factor 1.41) covers the T ranges shown in the second row of Fig. 3. The low T limit is extended. The first gap in row 1 is nicely covered, but the second is only partially

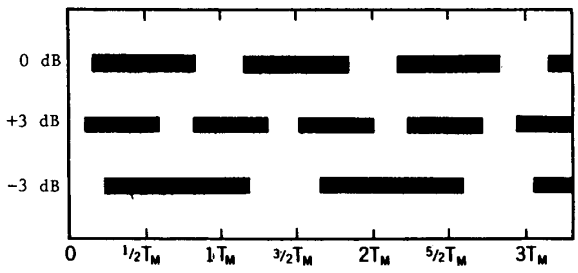

Fig. 3 Regions of T for which $\sin^2 aT > 0.25$ for three different a values. The scale is in units of T_m for optimum power.

covered. Data taken at a power level 3 dB below optimum (b smaller by a factor .71) covers the first two gaps in row 1. Data taken at all three powers gives multiple coverage at most T values. There will always be a gap at small values of T. But $\rho(T)$ vanishes there since small T values correspond to large velocities which are strongly cut off by a Maxwell distribution in the source. Three powers seem adequate to cover most distributions. Other choices of relative powers can also be used.

We can combine the data from several microwave powers as follows. Let the index j denote the power level. From each measured Ramsey fringe pattern $R_j(\lambda)$ we obtain a Fourier transform $F_j(T)$. We define trial distributions by

$$\rho_j(T) = F_j(T)/\sin^2 a_j T. \qquad (4)$$

These trial distributions usually differ from each other. For a best estimate of $\rho(T)$ we form a weighted average of the trial distributions:

$$\bar{\rho}(T) = \Sigma_j \rho_j(T) W_j(T) / \Sigma_j W_j(T). \qquad (5)$$

For a weight function we choose $W_j(T) = \sin^4 a_j T$, the square of the Rabi excitation probability. This weight function strongly suppresses contributions to $\bar{\rho}$ when $\sin^2 aT$ is not near unity. To avoid contributions to $\bar{\rho}$ from unphysical spikes in ρ_j like those shown in Fig. 2, we also set the weight function completely to zero whenever it is less than a cutoff value W_c. This zeroing of W_j implements the regions illustrated in Fig. 3. The $\sin^4 aT$ dependence softens the cutoff edge by making W_j small near the cutoff.

To get a measure of how closely the $\rho_j(T)$ do agree with each other, we introduce a quality-of-fit criterion

$$E(a) = \int_0^\infty D(T)\, dT, \qquad (6)$$

where $D(T) = \Sigma_j [\rho_j(T) - \bar{\rho}(T)]^2 W_j(T)$

is the mean square deviation of ρ_j from $\bar{\rho}$ at each T value, weighted by $W_j(T)$. Our choice of weight function makes E equivalent to the sum of the mean

square errors between the input lineshapes $R_j(\lambda)$ and lineshapes computed from the fitted distribution $\bar{\rho}(T)$.

The quality-of-fit criterion provides the solution to our second problem, the unknown a_j. If the ratios of powers are known, we can assume the ratios of a_j's are known. Then only one absolute value, say a_1, need be determined. If we try different values of a_1, or $T_m = \pi/a_1$, adjust the other a_j's in their proper ratio, and compute E, we find the dependence shown in Fig. 4. The minimum is more than two orders of magnitude deep and defines T_m within 0.5%.

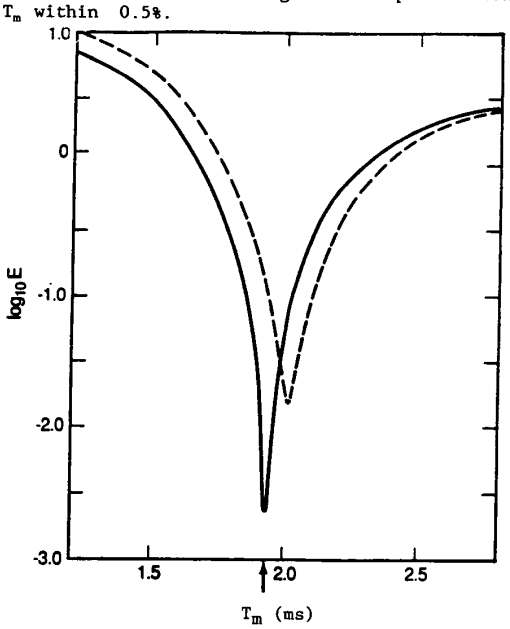

Fig. 4 Variation of E with trial values of T_m for theoretical lineshape data. The broken curve is without the ℓ/L correction and the solid curve is with the correction. The arrow points to the theoretical T_m value.

C. Summary of Method

To use our method we first obtain Ramsey fringe data $R_j(\lambda)$ at three or more power levels of known ratio ranging both above and below optimum power. Such a data set is shown in Fig. 5 for the full thermal distribution emerging from an oven. Numerical Fourier cosine transforms $F_j(T)$ are computed at each power level (Fig. 6). From the position of the first minimum in Fig. 6b a trial value for T_m is obtained. From it we obtain trial values for a_j and $W_j(T)$. We then evaluate $\bar{\rho}$ and E according to Eqs (4), (5), and (6). The value of T_m is then varied and the computations repeated until a minimum in E is obtained (Fig. 4). Finally the distribution is normalized so that

$$\int_0^\infty \bar{\rho}(T)\, dT = 1.$$

The fitted distribution $\bar{\rho}$ thus obtained from the data in Fig. 5 is shown in Fig. 7, along with the actual distribution used to generate the data. The agreement is good except for a systematic shift of $\bar{\rho}$ to higher T values. The minimum in Fig. 4 is also too high. Varying W_c from 0.025 to 0.250 produces little change in $\bar{\rho}$, so the fit is insensitive to this cutoff.

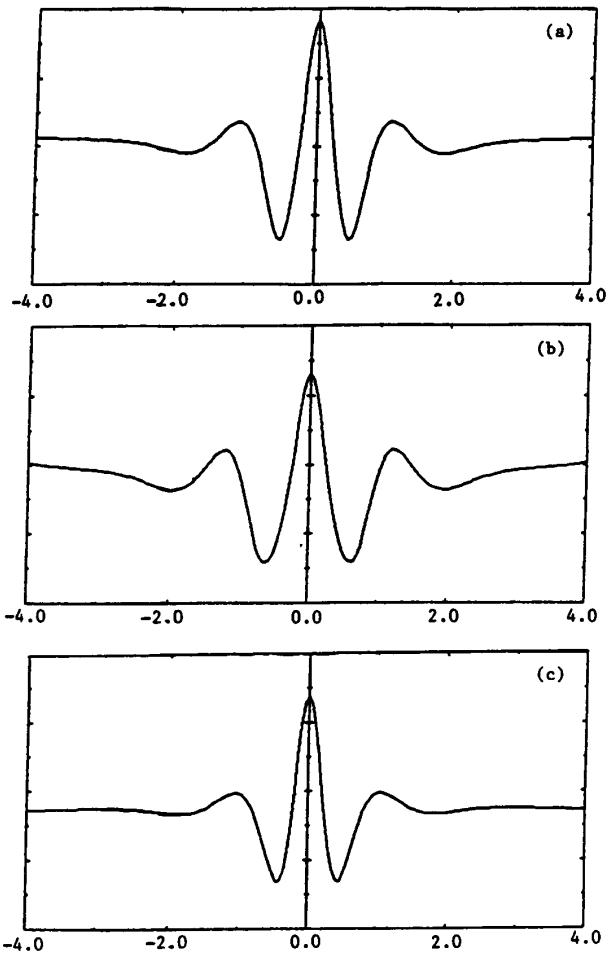

Fig. 5 Ramsey fringe lineshapes for full thermal distribution. (a) Optimum power. (b) 3 dB above optimum power. (c) 3 dB below optimum power. The horizontal scales are λ in kHz. L = 25 cm, ℓ = 1 cm and α = 251.3 m/sec.

III. First Order ℓ/L Corrections

Tests on data for other ℓ/L ratios show that the shifts in both Fig. 4 and Fig. 7 are proportional to ℓ/L. Daams's analysis [6] included first-order corrections in ℓ/L. We have done a similar analysis and find the following expression to replace (4):

$$\rho_j(T) = \frac{F_j(T) + b_j^{-1}\, G(b_j r)\, dF_j/dT}{\sin^2 a_j T[1-(\ell/L)G'(b_j r)]} \qquad (7)$$

To first order the numerator is equivalent to $F_j(T + G/b_j)$ explaining the shifts in Fig. 7. The function G depends on the microwave field profile seen by atoms as they traverse the excitation region. For a rectangular excitation field profile, found in most standards with transverse C-fields, we have

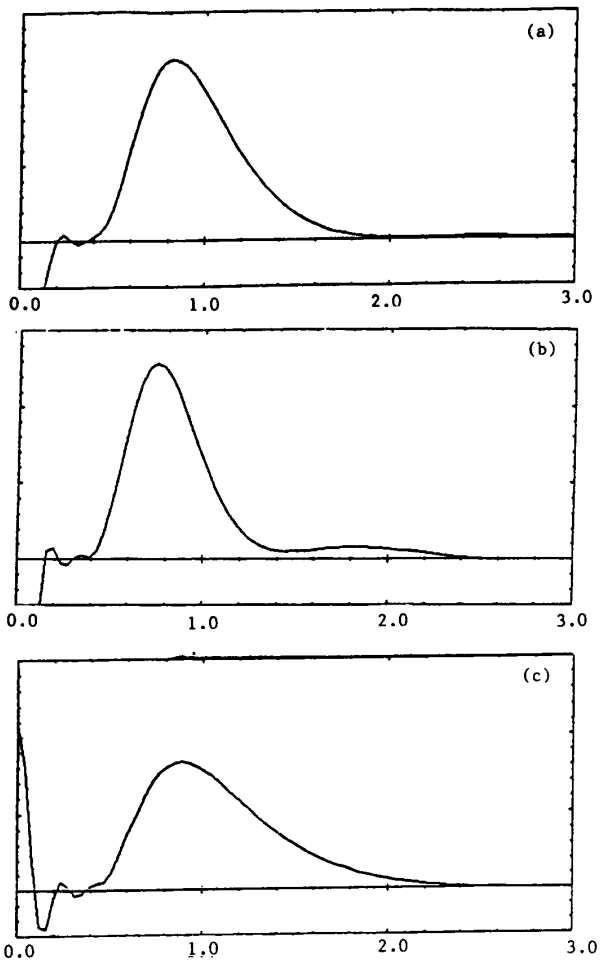

Fig. 6 Fourier transforms of the lineshapes in Fig. 5. (a) Optimum power. (b) 3 dB above optimum power. (c) 3 dB below optimum power. The horizontal scales are T in ms. The small T behavior arises from the Rabi pedestal.

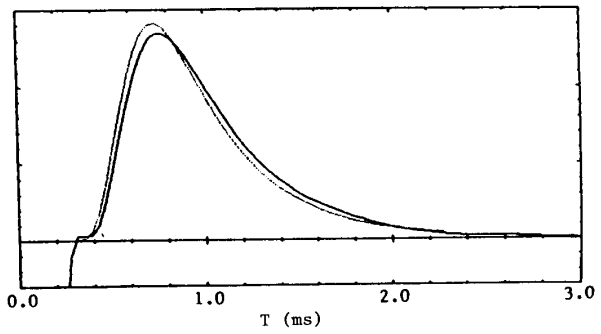

Fig. 7 Comparison of fitted distribution $\tilde{\rho}(T)$ (solid curve) with input thermal distribution (dotted curve) for $\ell/L = 0.04$ and no ℓ/L correction.

$$G_t(b\tau) = \tan b\tau.$$

For a half-sine-wave field profile, found in most standards with longitudinal C-fields, we have

$$G_s(b\tau) = b\tau \sec b\tau \, J_0(b\tau).$$

G′ is the derivative of G with respect to its argument $b\tau$. For $T \leq \frac{1}{2}T_m$ we have $G/b \approx \tau$ and $G' \approx 1$ for either profile.

When the first order ℓ/L corrections in (7) were included in the computer program, we obtained the fit shown in Fig. 8. The shift has disappeared and only small discrepancies remain. The quality-of-fit criterion, shown by the solid curve in Fig. 4, has a minimum smaller by a factor 8 and only 0.3% from the correct value of T_m.

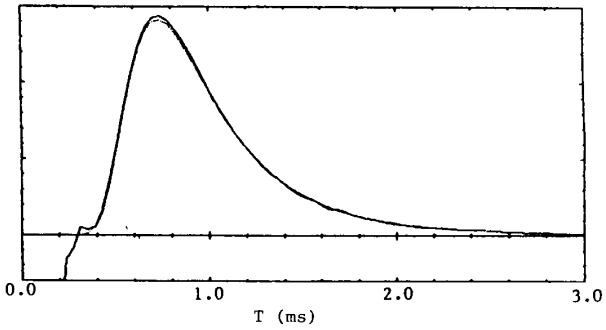

Fig. 8 Comparison of fitted distribution $\tilde{\rho}(T)$ (dotted curve) with input thermal distribution (solid curve) for $\ell/L = 0.04$ with ℓ/L correction.

IV. Test on Experimental Data

In Fig. 9 we show a set of experimental Ramsey curves for the primary frequency standard NBS-4 [8]. The wings of the curves show the shape of the underlying Rabi pedestal. The first two side lobes on each side are nearly the same height, while the next ones are weaker. Irregularities in the periodicity of the side lobes are also apparent in all three lineshapes. Such features hold information about the velocity distribution which a Fourier transform can reveal.

Figure 10 shows the transit-time distribution obtained by our method from the lineshapes in Fig. 9. The distribution is separated into two well-resolved parts. Each part produces a Ramsey fringe with its own oscillation frequency for the side lobes. The beating of these two frequencies accounts for most of the unusual features seen in Fig. 9, especially the phase change in the third side lobe (first side lobe at the +3 dB power level). The narrow dip separating the parts in Fig. 10 is responsible for the large number of weak side lobes. This dip is probably caused by a narrow obstruction in the beam tube which physically blocks a class of atomic trajectories spanning a limited velocity range. In Fig. 11 the transit-time distribution has been converted to a velocity distribution by the relation

$$\sigma(v) = (L/v^2)\rho(L/v).$$

This distribution is very similar to one obtained previously [8, Fig. 16] by a pulse method [3].

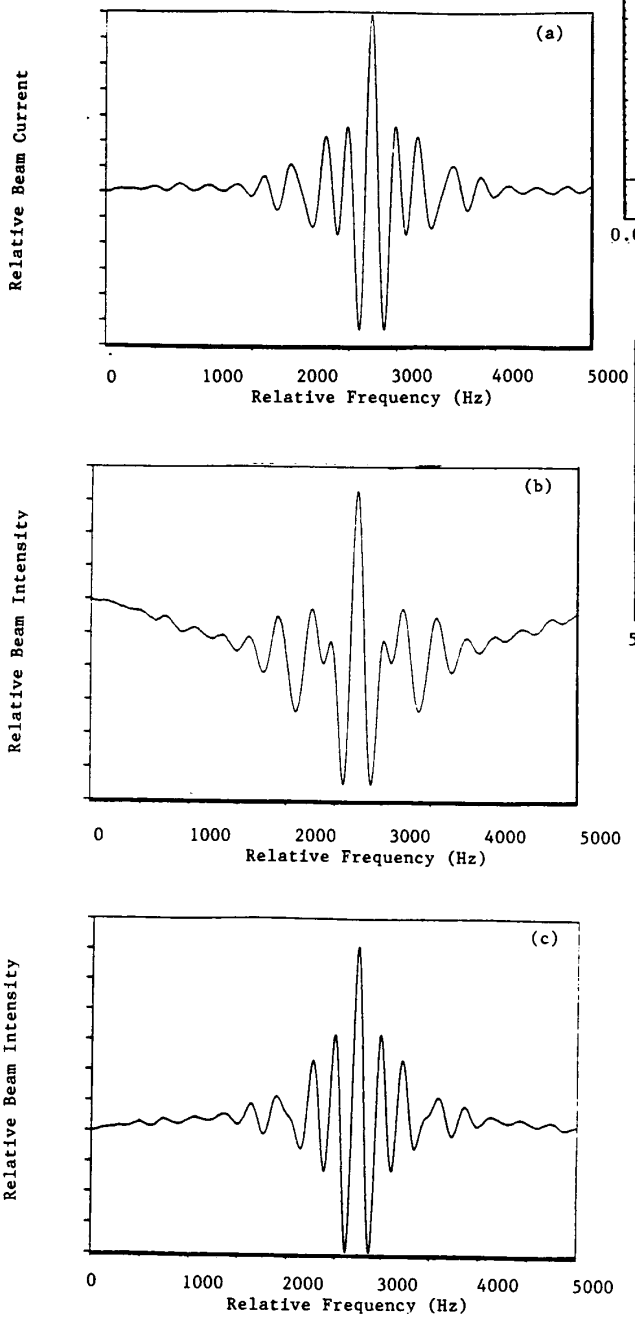

Fig. 9 Ramsey fringe lineshapes for the primary frequency standard NBS-4. (a) Optimum power. (b) 3dB above optimum power. (c) 3 dB below optimum power.

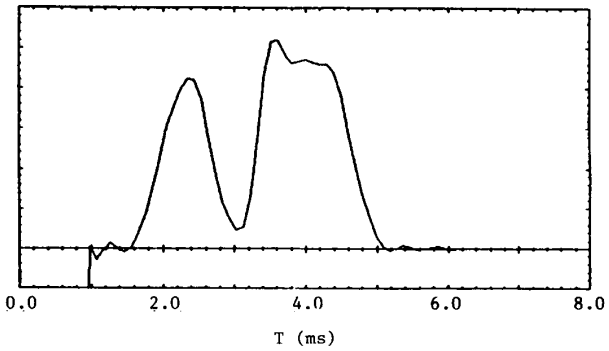

Fig. 10 Fitted transit-time distribution for the primary frequency standard NBS-4.

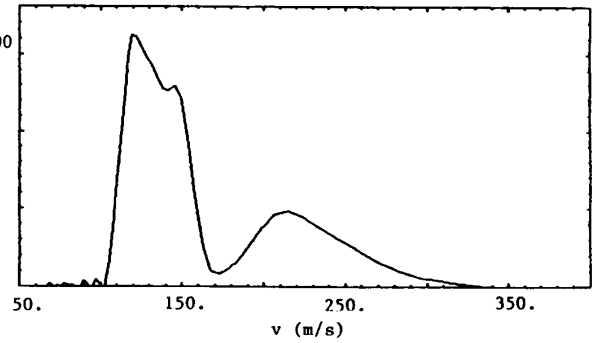

Fig. 11 Fitted velocity distribution for the primary frequency standard NBS-4.

V. Summary

We have developed a method that starts with the Fourier cosine transforms of Ramsey lineshapes and extracts from them a transit-time distribution $\rho(T)$. The method includes first order ℓ/L corrections and a quality-of-fit criterion that enables the power parameter b to be accurately determined. By testing the method on theoretically generated data we have shown it capable of finding distributions accurate within a few percent for $\ell/L = 0.04$. Analysis of theoretical lineshapes with $\ell/L = 0.01$ have produced fits that agree with the input distribution to 1% for a narrow, two-peaked distribution, and 0.1% for the broad thermal distribution. Hence our method can provide velocity distributions with accuracy sufficient to meet the anticipated needs of optically pumped primary standards.

References

[1] R. E. Drullinger, "Frequency Standards Based on Optically Pumped Cesium," Proc. IEEE 74, 140 (1986) and references therein.

[2] A. De Marchi, G. D. Rovera, and A. Premoli, "Pulling by Neighbouring Transitions and Its Effects on the Performance of Caesium-Beam Frequency Standards," Metrologia 20, 530 (1984).

[3] H. Hellwig, S. Jarvis, D. Halford, and H. E. Bell, "Evaluation and Operation of Atomic Beam Tube Frequency Standards Using Time

Domain Velocity Selection Modulation," Metrologia 9, 107 (1973).

[4] J.-S. Boulanger, "A New Method for the Determination of Velocity Distributions in Cesium Beam Clocks," Metrologia 23, 37 (1986).

[5] S. Jarvis, "Determination of Velocity Distributions in Molecular Beam Frequency Standards from Measured Resonance Curves," Metrologia 10, 87 (1974).

[6] H. Daams, "Corrections for Second-Order Doppler Shift and Cavity Phase Error in Cesium Atomic Beam Frequency Standards," IEEE Trans. Inst. Meas. IM-23, 509 (1974).

[7] N. F. Ramsey, Molecular Beams, Oxford University Press (1956).

[8] D. J. Glaze, H. Hellwig, D. W. Allan, S. Jarvis, Jr., and A. E. Wainwright, "Accuracy Evaluation and Stability of the NBS Primary Frequency Standards," IEEE Trans. Inst. Meas. IM-23, 489 (1974).